Improved Compressive, Damping and Coefficient of Thermal Expansion Response of Mg–3Al–2.5La Alloy Using Y$_2$O$_3$ Nano Reinforcement

Amit Kumar [1], Khin Sandar Tun [1], Amit Devendra Kohadkar [2] and Manoj Gupta [1,*]

[1] Department of Mechanical Engineering, National University of Singapore, 9 Engineering Drive 1, Singapore 117576, Singapore; amittonk@gmail.com (A.K.); mpekhst@nus.edu.sg (K.S.T.)
[2] Department of Mechanical engineering, Visvesvaraya National Institute of Technology, South Ambazari Road, Nagpur 440010, India; amitkohadkar@gmail.com
[*] Correspondence: mpegm@nus.edu.sg; Tel.: +65-6516-6358

Abstract: In the present study, the effects of the addition of Y$_2$O$_3$ nanoparticles on Mg–3Al–2.5La alloy were investigated. Materials were synthesized using a disintegrated melt deposition technique followed by hot extrusion. The samples were then characterized for microstructure, compression properties, damping properties, CTE (coefficient of thermal expansion) and fracture morphology. The grain size of Mg–3Al–2.5La was significantly reduced by the addition of the Y$_2$O$_3$ nano-sized reinforcement (~3.6 μm, 43% of Mg–3Al–2.5La grain size). SEM and X-ray studies revealed that the size of uniformly distributed intermetallic phases, Al$_{11}$La$_3$, Al$_2$La, and Al$_{2.12}$La$_{0.88}$ reduced by the addition of Y$_2$O$_3$ to Mg–3Al–2.5La alloy. The coefficient of thermal expansion (CTE) was slightly improved by the addition of nanoparticles. The results of the damping measurement revealed that the damping capacity of the Mg–3Al–2.5La alloy increased due to the presence of Y$_2$O$_3$. The compression results showed that the addition of Y$_2$O$_3$ to Mg–3Al–2.5La improved the compressive yield strength (from ~141 MPa to ~156 MPa) and the ultimate compressive strength (from ~456 MPa to ~520 MPa), which are superior than those of the Mg–3Al alloy (Compressive Yield Strength, CYS ~154 MPa and Ultimate Compressive Strength, UCS ~481 MPa). The results further revealed that there is no significant effect on the fracture strain value of Mg–3Al–2.5La due to the addition of Y$_2$O$_3$.

Keywords: Mg–Al–RE alloy; magnesium alloy; damping; Al$_{11}$La$_3$ phase; nanosize reinforcement; mechanical properties

1. Introduction

Mg–Al-based alloys are considered important lightweight alloys due to their low density, high strength, and stiffness with good casting and processing ability. Although Mg–Al alloys exhibit a superior combination of mechanical properties, they are not suitable for application in automobile engine components due to their poor creep resistance [1,2]. It is well reported that poor creep properties in Mg–Al alloys are due to the formation of the β-eutectic phase (Mg$_{17}$Al$_{12}$), which is unstable at high temperatures [3]. To improve the creep properties of Mg–Al, rare earth metals (RE) were used as alloying elements, as they can suppress the formation of the β-phase. In addition, RE also improved the grain refinement and strength while retaining the ductility, creep resistance, corrosion resistance and fatigue strength [4–7]. The addition of lanthanum (La) to Mg–4Al exhibited a good strengthening effect due to its precipitation hardening and grain refinement effects [3]. In our recent study on Mg–3Al–*x*La (*x* = 1%, 2.5% and 4%), it was observed that the addition of La to Mg–3Al led to the consumption of most of the Al for the formation of Al$_{11}$La$_3$, Al$_2$La, and Al$_{2.12}$La$_{0.88}$ intermetallic phases and

suppressed the formation of the $Mg_{17}Al_{12}$ phase [8]. Among all the compositions, the Mg–3Al–2.5La alloy exhibited the best tensile properties; Tensile Yield Strength, TYS ~160 MPa, Ultimate Tensile Strength, UTS ~249 MPa and fracture strain ~22%. However, the addition of La in Mg–3Al alloy caused a gradual decrease in the compressive strength and elongation [8].

On the other hand, nano-sized reinforcement (thermally stable ceramics such as Al_2O_3, ZrO_2, Y_2O_3) used in magnesium-based nanocomposites has already shown potential improvement in the mechanical properties and ductility without any significant increase in the density [9–13]. Many types of advanced metal matrix nanocomposites are now easily available, and they exhibit functional properties. Recently, a few particle-reinforced, self-lubricating and self-healing metal matrix nanocomposites were synthesized using solidification techniques [14–16]. Hassan et al. [17] showed that the addition of nano-sized yttrium oxide (Y_2O_3) particulates as a reinforcement in magnesium, synthesized by the disintegrated melt deposition (DMD) technique, enhanced the mechanical properties of the magnesium matrix. This work concluded that the addition of 1.9% Y_2O_3 by weight exhibits the best mechanical properties compared to 0.6% and 3.1% Y_2O_3 [17].

The present work addresses the further enhancement of the compression and damping response of Mg–3Al–2.5La alloy using Y_2O_3 nano particulates as a reinforcement. Mg–3Al–2.5La alloy, containing 1.9% Y_2O_3 by weight as reinforcement, is synthesized along with pure Mg, Mg–3Al and Mg–3Al–2.5La alloys, using the Disintegrated Melt Deposition (DMD) technique followed by hot extrusion. A detailed view of the effect of the Y_2O_3 addition on the microstructure, Coefficient of Thermal Expansion (CTE), compression and damping properties of Mg–3Al–2.5La is provided.

2. Materials and Characterizations

2.1. Materials

Magnesium turnings (99.9% purity) supplied by Acros Organics (Geel, Belgium) were used as the base material. Aluminium powder (99% purity) of size ~7–15 μm supplied by Alfa Aesar (Haverhill, MA, USA) and Mg–30%La master alloy supplied by Sunreiler Metal Co. Limited (Beijing, China) were used as alloying elements. Yttrium oxide (99.995% purity) of size 20–40 nm supplied by US Research Nanomaterials (Houston, TX, USA) was used as reinforcement in this study.

2.2. Processing

Four different compositions, pure Mg, Mg–3%Al, Mg–3%Al–2.5%La and Mg–3%Al–2.5%La–1.9%Y_2O_3 by weight were synthesized using disintegrated melt deposition technique [18]. Pure Mg turnings, Al powder, Y_2O_3 powder and Mg–30%La master alloy were placed in a multilayered sandwich fashion in a graphite crucible and superheated to 750 °C under an argon gas atmosphere using electrical resistance furnace (Dakin Engineering Pte Ltd., Singapore). For uniform distribution of reinforcement particulates within the alloy matrix, the superheated slurry was then stirred at 450 rpm for 5 min using a stainless steel impeller (Starlight Tool Precision Engineering, Singapore) with twin blade (pitch 45°). Stainless steel stirrer was used to avoid any iron contamination of the molten metal. After stirring, the molten melt was down poured through a nozzle of 10 mm diameter at the bottom of the crucible to the mould under the influence of gravity. Before entering the mold, the molten metal was disintegrated by two jets of argon gas, oriented normal to the melt stream. The flow of argon was maintained at 25 L/min [17]. An ingot of 40 mm diameter was then obtained. For synthesizing other compositions similar steps were followed. As cast ingot was later machined to 36 mm diameter and 45 mm length for the secondary processing.

Secondary processing involved the soaking of ingot at 400 °C for 1 h in a constant temperature furnace (Elite Thermal Systems Ltd., Market Harborough, Leicestershire, UK). Using a 150-ton hydraulic extrusion press, hot extrusion was carried out at 350 °C die temperature with an extrusion ratio of 20.25:1 to obtain rods of 8 mm diameter. Extruded rods were further used to prepare samples for different characterization studies.

2.3. Characterizations

2.3.1. Microstructural Characterization

The microstructure was characterized using an optical microscope (Olympus Corporation, Shinjuku, Tokyo, Japan) on polished and etched samples (etchant: 4.2 gm picric acid, 10 mL acetic acid, 70 mL ethanol and 10 mL distilled water). The grain size was measured on the longitudinal section of samples, with the help of Scion image analysis software (beta 4.0.2, Frederick, MD, USA, 2000). To observe intermetallic phase formation and distribution, scanning electron microscopes JEOL JSM-6010 (JEOL Ltd., Tokyo, Japan) and Hitachi FESEM-S4300 (Hitachi, Ltd., Tokyo, Japan) equipped with energy dispersive spectrometric analysis (EDS) were used. X-Ray diffraction analysis was conducted using an automated Shimadzu LAB-XRD-6000 (Shimadzu Corporation, Kyoto, Japan) (Cu Kα:λ = 1.54056 Å) spectrometer with a scan speed of 2$°$/min.

2.3.2. Physical Characterization

Density and Porosity: The density of extruded pure Mg, Mg–3%Al, Mg–3%Al–2.5%La and Mg–3%Al–2.5%La–1.9%Y_2O_3 was measured using a gas pycnometer (Micromeritics Instrument Corp., Norcross, GR, USA). Each sample was run for five cycles to measure the density more accurately. Pure helium gas was purged with a pressure of 19.5 Psig for all the five cycles with a cycle fill pressure of 19.5 Psig. The difference between theoretical density (calculated by the rule of mixture) and experimentally measured density was quantified as the porosity level in the material.

The Coefficient of thermal expansion: By using a thermo-mechanical analysis instrument LINSEIS TMA PT 1000LT (Linseis Thermal Analysis, Robbinsville, NJ, USA) the coefficient of thermal expansion (CTE) of pure Mg, Mg–3%Al, Mg–3%Al–2.5%La and Mg–3%Al–2.5%La–1.9%Y_2O_3 was determined. The heating rate of 5 $°$C/min was maintained with constant argon flow rate of 0.1 L per minute. The displacement of the test samples (each of 5 mm length and 8 mm diameter) was measured as a function of temperature (323 K to 673 K) using an alumina probe (Linseis Thermal Analysis, Robbinsville, NJ, USA).

Damping: The vibrational damping capacity of the materials was measured using the resonance frequency damping analyzer (RFDA), (IMEC, Genk, Belgium). The vibration signal of each material (8 mm diameter, 60 mm length) was measured as a function of amplitude vs. time.

2.3.3. Mechanical Characterization

Compression Properties: In accordance with ASTM E9-09, compressive properties of extruded pure Mg, Mg–3%Al, Mg–3%Al–2.5%La and Mg–3%Al–2.5%La–1.9%Y_2O_3 samples were determined at ambient temperature, using a fully automated servo-hydraulic mechanical testing machine, MTS-810 (MTS systems corporation, Eden Prairie, MN, USA). The compression properties were measured at a strain rate of 8.334×10^{-5} s^{-1}. The specimens of 8 mm diameter, with length to diameter ratio of one were used. At least five different samples of each composition were tested to ensure repeatability of results. Fractured surfaces of all samples were analyzed using Hitachi S-4300 FESEM (Hitachi, Ltd., Tokyo, Japan).
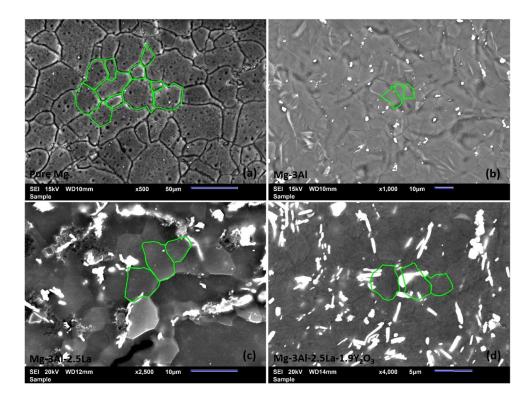
3. Results and Discussion

3.1. Microstructural Characterization

The microstructures of all the samples were initially characterized using SEM microscopy (JEOL Ltd., Tokyo, Japan) (Figure 1). Table 1 and Figure 2a show the grain size of different compositions after analysis. The results revealed that the addition of 2.5% La and 1.9% Y_2O_3 to Mg–3Al reduced the average grain size by ~50%. It was observed that the addition of Al in Mg (Figure 1a,b) significantly reduced the grain size from ~22.6 μm to ~7.74 μm. It is frequently reported that during the solidification of Mg–Al alloys, fine grains are nucleated as the primary-Mg solid solution, along with

the $Mg_{17}Al_{12}$ eutectic mixture distributed along the grain boundaries [1,2,19,20]. Secondary processing or hot deformation during extrusion further breaks down the $Mg_{17}Al_{12}$ network structure into fine precipitates, which results in grain refinement as observed in Mg–3Al (Figure 1b). Hot extrusion was performed at 350 °C (which is >0.5 T_m of pure Mg), and therefore it resulted in recrystallization and the formation of nearly equiaxed grains.
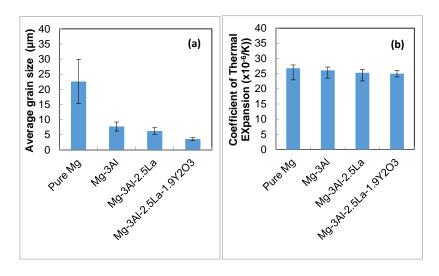
As the solubility of La in Mg is very limited (~0.78 wt %) [21,22] and La is a grain refiner, therefore the addition of 2.5% La to Mg–3Al alloy further reduced the average grain size from ~7.74 μm to ~6.26 μm. These results obtained in this study are in good agreement with other available reports claiming La as an excellent grain refiner in Mg [23,24]. The reinforcement of nano-sized thermally stable 1.9% Y_2O_3 powder to Mg–3Al–2.5La further reduced the grain size as Y_2O_3 nanoparticles can act as the nucleation sites during solidification and recrystallization besides pinning the grain boundaries in the later stages. Figure 2a represents the change in the grain size of pure Mg with the addition of 3Al, 2.5La, and 1.9Y_2O_3 subsequently.

Figure 1. Scanning Electron Microscopic (SEM) micrographs of (**a**) pure Mg, (**b**) Mg–3Al, (**c**) Mg–3Al–2.5La, and (**d**) Mg–3Al–2.5La–1.9Y_2O_3 alloys, illustrating the grain structure.
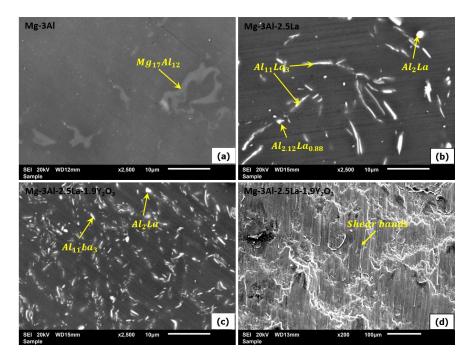
Table 1. Results of average grain size, density, porosity and Coefficient of Thermal Expansion (CTE) measurements.

Material (wt %)	Average Grain Size (μm)	Density and Porosity Measurements			CTE ($\times 10^{-6}$/K)
		Theoretical Density (g/cc)	Experimental Density (g/cc)	Porosity (%)	
Pure Mg	22.6 ± 7.3	1.738	1.737	0.15	26.8 ± 3.9
Mg–3Al	7.74 ± 1.5	1.758	1.753	0.29	26.1 ± 2.6
Mg–3Al–2.5La	6.26 ± 1.1	1.791	1.788	0.17	25.3 ± 2.7
Mg–3Al–2.5La–1.9Y_2O_3	3.6 ± 0.5	1.818	1.813	0.16	25.0 ± 1.1

Figure 2. Change in (**a**) grain size and (**b**) coefficient of thermal expansion in pure Mg with the addition of 3Al, 2.5La and $1.9Y_2O_3$ subsequently.

Figure 3a–c are the SEM micrographs of Mg–3Al, Mg–3Al–2.5La, and Mg–3Al–2.5La–$1.9Y_2O_3$ alloys. Figure 3a–b show the SEM micrographs of extruded Mg–3Al and Mg–3Al–2.5La alloys. In Mg–3Al alloy, the dispersed $Mg_{17}Al_{12}$ phase is distributed inside the Mg matrix. A uniformly distributed bright white phase appeared in the Mg–3Al–2.5La alloy (Figure 3b) in rod-like ($Al_{11}La_3$) and polygon-type (Al_2La, $Al_{2.12}La_{0.88}$) shapes, which is consistent with earlier reports [3,21,25–29]. The brighter second phase in Figure 3c is broken into even finer shapes in the Mg–3Al–2.5La–$1.9Y_2O_3$ alloy, especially rod-like shapes, illustrating the ability of Y_2O_3 nanoparticles to refine the second phases. Similar findings were observed as a result of the addition of Al_2O_3 in the AZ31 alloy [30]. The uniform distribution of the second phase is due to the hot extrusion, which broke down these scattered rod-like and polygon shapes into small pieces throughout the microstructure.

Figure 3. SEM micrographs of (**a**) Mg–3Al, (**b**) Mg–3Al–2.5La, and (**c**) Mg–3Al–2.5La–$1.9Y_2O_3$ alloys; (**d**) compressive fractograph of Mg–3Al–2.5La–$1.9Y_2O_3$ alloys.

X-ray diffraction (XRD) studies conducted in the longitudinal direction of the samples are shown in Figure 4. These diffractograms did not reveal the presence of any La phase with Mg, which is consistent with other available reports on Mg–Al–La alloys [8,21,22,25–29,31,32]. However, they revealed the strong presence of Mg peaks together with the phase comprised of $Al_{11}La_3$, Al_2La and $Al_{2.12}La_{0.88}$, which are also observed in the SEM micrographs. The formation of $Al_{11}La_3$, Al_2La and $Al_{2.12}La_{0.88}$ as intermetallic phases occurred due to the large difference in the electronegativity of Al and La when compared to Mg and Al [21,33,34]. It is well documented in the literature that dominating diffraction angles in extruded Mg rods corresponding to $2\theta = 32°$, $34°$ and $36°$, respectively, represent the prismatic $(1, 0, -1, 0)$ plane, the basal $(0, 0, 2, 0)$ plane and the pyramidal $(1, 0, -1, 0)$ plane of HCP Mg crystal [35]. From the intensity of these peaks at various diffraction angles, it is evident that the addition of La in Mg–3Al increased the I/I_{max} ratio for the basal plane but the pyramidal texture still dominated. The Mg–3Al–2.5La–1.9Y_2O_3 alloy showed that the peak corresponding to the basal plane becomes dominant. This indicates that the presence of Y_2O_3 clearly strengthens the basal texture in the Mg–3Al–2.5La alloy.
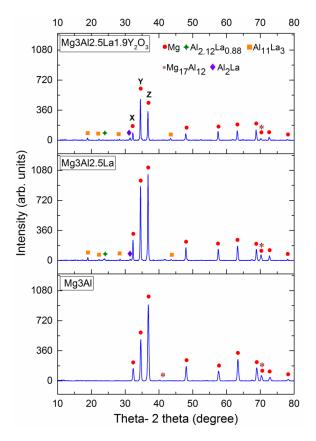

Figure 4. X-ray diffraction results of Mg–3Al, Mg–3Al–2.5La and Mg–3Al–2.5La–1.9Y_2O_3 alloys.

3.2. Physical Characterization

3.2.1. Density and Porosity

From Table 1, it is observed that near-dense Mg materials were synthesized utilizing the disintegrated melt deposition technique coupled with hot extrusion. The experimentally measured density values of the synthesized alloys and composite are closer to those of theoretically calculated density values. The increase in the density values of pure Mg was due to the addition of relatively high-density Al, La and Y_2O_3 elements when compared to pure magnesium.

The volumetric porosity results, which were calculated using theoretical and experimental density values, show that the addition of Y_2O_3 did not affect the porosity of the base Mg–3Al–2.5La alloy.

3.2.2. The Coefficient of Thermal Expansion

Table 1 and Figure 2b show the results of the coefficient of thermal expansion (CTE) measurements within the 25–400 °C temperature range. The results show that the CTE value of pure magnesium decreased with the alloying additions of Al, La and Y_2O_3. The gradual decrease in the CTE values of Mg, Mg–3Al, Mg–3Al–2.5La and Mg–3Al–2.5La–1.9Y_2O_3 alloy was due to the presence of the alloying addition of Al, La and Y_2O_3 which have lower CTE values (23.1×10^{-6}/K, 12.1×10^{-6}/K and 8.1×10^{-6}/K) as compared to pure Mg (26.8×10^{-6}/K) [36]. The results (see Figure 2b) suggest that the alloys and nanocomposites investigated in this study are more dimensionally stable with respect to temperature when compared to pure Mg.

3.2.3. Damping

The damping characteristics of extruded pure Mg, Mg–3Al, Mg–3Al–2.5La and Mg–3Al–2.5La–1.9Y_2O_3 alloys are presented in Table 2. The damping capacity of a material is defined as the ability to absorb vibration. The value of the damping capacity of a material depends on its properties such as density, microstructure, and elasticity [8,37]. The results show that the damping capacity of pure Mg decreased with the addition of Al in Mg–3Al, which was further enhanced by the addition of 2.5La in Mg–3Al–2.5La. The addition of Y_2O_3 further improved the damping capacity of the Mg–3Al–2.5La.
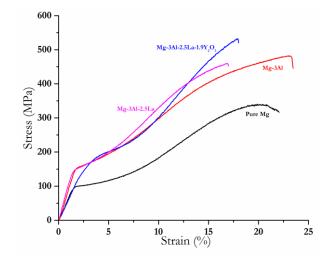
The damping loss rate represents how fast a material stops vibration. The results indicate that addition of 1.9% Y_2O_3 decreased the damping loss rate compared to the addition of 2.5% La. The significant change in the damping properties of alloys can be due to the damping mechanisms related to texture reorientation, thermal mismatch, defects, porosity, dislocation and grain boundary.

Table 2. Room-temperature compressive and damping properties of pure Mg, Mg–3Al, Mg–3Al–2.5La and Mg–3Al–2.5La–1.9Y_2O_3 alloys.

Material	0.2% CYS (MPa)	UCS (MPa)	Fracture Strain (%)	Damping Loss Rate	Damping Capacity
Pure Mg [8]	90 ± 6	333 ± 4	23 ± 0.74	8.00 ± 1.000	0.000456
Mg–3Al [8]	154 ± 2	481 ± 7	24 ± 0.5	6.16 ± 0.377	0.000204
Mg–3Al–2.5La [8]	141 ± 4	456 ± 3	18 ± 1	8.29 ± 0.827	0.000265
Mg–3Al–2.5La–1.9Y_2O_3	156 ± 5	520 ± 8	18 ± 0.70	7.60 ± 0.701	0.000272

3.3. Mechanical Characterization

Compression properties: Table 2 and Figure 5 show the room-temperature compression properties of extruded pure Mg, Mg–3Al, Mg–3Al–2.5La and Mg–3Al–2.5La–1.9Y_2O_3 samples under compression loading. As evident from the results, the addition of 3Al in pure Mg enhanced the compressive yield strength (CYS), the ultimate compressive strength (UCS) and the fracture strain (FS) from ~90 MPa, ~333 MPa and ~23% to a level of ~154 MPa, ~481 MPa and ~24%. This increase in compressive strength was due to the hall-patch effect as there was a tremendous (~73%, ~22.6 μm to ~7.76 μm) reduction in grain size of the pure Mg. Another possible reason is the presence of fine $Mg_{17}Al_{12}$ precipitates near the grain boundaries, which lead to precipitation hardening. The addition of 2.5La to Mg–3Al significantly reduced the CYS, UCS and failure strain values. In spite of the grain refinement (~7.74 μm to ~6.26 μm), the compression strength of Mg–3Al–2.5La decreased. This was due to the presence of intermetallic Al_2La and $Al_{2.12}La_{0.88}$ with fine $Al_{11}La_3$ phases, which are hard and exhibit sharp edges. Stress concentrates on these sharp edges and causes early crack initiation and subsequent crack propagation. The addition of nano-sized reinforcement particulates of Y_2O_3 further refined the grain size of Mg-3Al-2.5La (~6.26 μm to ~3.6 μm) and fragmented the second phases, resulting in the best improvement of the CYS and UCS.

Figure 5. Stress-strain curves of extruded pure Mg, Mg–3Al, Mg–3Al–2.5La and Mg–3Al–2.5La–1.9 Y_2O_3 alloys under compression loading.

The presence of finer secondary phases assisted in restricting the motion of dislocations more effectively, leading to strength improvement in the case of the nanocomposite. Overall, the fracture strain remained unaffected (~18%) by the addition of the reinforcement when compared to the base alloy. Therefore, the addition of nano-sized Y_2O_3 compensated for the decrease in the compression strength of Mg–3Al due to the addition of 2.5La, while the presence of La suppressed the formation of the $Mg_{17}Al_{12}$ phase, which adversely affects the creep properties of Mg–3Al alloys.

The compression fracture morphology of the Mg–3Al–2.5La–1.9Y_2O_3 alloy is shown in Figure 3d. Compressive fractography studies (quasi-static) showed that the materials underwent the shear mode of deformation with the addition of the reinforcement. The ample split into two parts and the fracture surfaces of all samples were inclined at an angle of ~45°. The SEM fractograph of fractured surfaces revealed the presence of shear bands in the sample. Smooth fracture surfaces exhibited a ductile mode of fracture in the samples [38,39].

4. Conclusions

In this work, the effect of the addition of Y_2O_3 on the microstructural and mechanical properties of Mg–3Al–2.5La alloy was primarily investigated. The following conclusions can be drawn:

1.　With the addition of the Y_2O_3 reinforcement, an even finer grain structure can be realized (~3.6 μm for Mg–3Al–2.5La–1.9 Y_2O_3 alloy, 43% less than that of Mg–3Al–2.5La at ~6.26 μm).
2.　The microstructural characterization concluded that all intermetallic phases Al_2La and $Al_{2.12}La_{0.88}$ and $Al_{11}La_3$ were still present in dispersed form, but the sizes of these phases were refined by the addition of nanosize Y_2O_3 in the Mg–3Al–2.5La alloy.
3.　The compressive results concluded that the addition of Y_2O_3 to Mg–3Al–2.5La significantly improved the compressive yield strength and the ultimate compressive strength (CYS from ~141 MPa to ~156 MPa and UCS from ~456 MPa to ~520 MPa), which are even better than those of the Mg–3Al alloy (CYS, ~154 MPa and UCS, ~481 MPa). There was no adverse effect on the fracture strain value recorded for Mg–3Al–2.5La with the addition of Y_2O_3.
4.　The damping results concluded that the addition of nanosize Y_2O_3 to Mg–3Al–2.5La improved the damping capacity. The addition of the Y_2O_3 reinforcement also improved the CTE value of the Mg–3Al–2.5La alloy.

Author Contributions: Amit Kumar and Amit Devendra Kohadkar performed processing; Amit Devendra Kohadkar performed mechanical testing; Amit Kumar and Khin Sandar Tun performed microstructure studies and data analysis; Amit Kumar wrote the paper; Manoj Gupta contributed consultation, data analysis and paper review.

Conflicts of Interest: The authors declare no conflict of interest.

References

1. Khomamizadeh, F.; Nami, B.; Khoshkhooei, S. Effect of rare-earth element additions on high-temperature mechanical properties of AZ91 magnesium alloy. *Metall. Mater. Trans. A* **2005**, *36*, 3489–3494. [CrossRef]

2. Braszczyńska-Malik, K.N. Precipitates of r–Mg17Al12 Phase in AZ91 Alloy. Available online: http://cdn.intechweb.org/pdfs/12741.pdf. (accessed on 14 March 2017).

3. Rokhlin, L.L. *Magnesium Alloys Containing Rare Earth Metals: Structure and Properties*; Crc Press: Florida, FL, USA, 2003.

4. Gupta, M.; Sharon, N.M.L. *Magnesium, Magnesium Alloys, and Magnesium Composites*; John Wiley & Sons: Hoboken, NJ, USA, 2011.

5. Mirzadeh, H. Constitutive analysis of Mg–Al–Zn magnesium alloys during hot deformation. *Mech. Mater.* **2014**, *77*, 80–85. [CrossRef]

6. Mirzadeh, H. Quantification of the strengthening effect of rare earth elements during hot deformation of Mg–Gd–Y–Zr magnesium alloy. *J. Mater. Res. Technol.* **2016**, *5*, 1–4. [CrossRef]

7. Hihara, L.H.; Adler, R.P.; Latanision, R.M. *Environmental Degradation of Advanced and Traditional Engineering Materials*; CRC Press: Florida, FL, USA, 2013.

8. Kumar, A.; Meenashisundaram, G.K.; Manakari, V.; Parande, G.; Gupta, M. Lanthanum effect on improving CTE, damping, hardness and tensile response of Mg–3Al alloy. *J. Alloy. Compd.* **2017**, *695*, 3612–3620. [CrossRef]

9. Hassan, S.; Gupta, M. Development of high performance magnesium nanocomposites using solidification processing route. *Mater. Sci. Technol.* **2004**, *20*, 1383–1388. [CrossRef]

10. Hassan, S.; Gupta, M. Effect of length scale of Al2O3 particulates on microstructural and tensile properties of elemental Mg. *Mater. Sci. Eng. A* **2006**, *425*, 22–27. [CrossRef]

11. Hassan, S.; Gupta, M. Effect of type of primary processing on the microstructure, CTE and mechanical properties of magnesium/alumina nanocomposites. *Compos. Struct.* **2006**, *72*, 19–26. [CrossRef]

12. Hassan, S.; Gupta, M. Development of high performance magnesium nano-composites using nano–Al2O3 as reinforcement. *Mater. Sci. Eng. A* **2005**, *392*, 163–168. [CrossRef]

13. Hassan, S.; Gupta, M. Effect of different types of nano-size oxide particulates on microstructural and mechanical properties of elemental Mg. *J. Mater. Sci.* **2006**, *41*, 2229–2236. [CrossRef]

14. Dorri Moghadam, A.; Ferguson, J.B.; Schultz, B.F.; Lopez, H.; Rohatgi, P.K. Direct Synthesis of Nanostructured in Situ Hybrid Aluminum Matrix Nanocomposite. *Ind. Eng. Chem. Res.* **2016**, *55*, 6345–6353. [CrossRef]

15. Moghadam, A.D.; Schultz, B.F.; Ferguson, J.B.; Omrani, E.; Rohatgi, P.K.; Gupta, N. Functional metal matrix composites: Self-lubricating, self-healing, and nanocomposites-an outlook. *JOM* **2014**, *66*, 872–881. [CrossRef]

16. Rohatgi, P.K.; Afsaneh, D.M.; Schultz, B.F.; Ferguson, J.B. Synthesis and Properties of Metal Matrix Nanocomposites (MMNCS), Syntactic Foams, Self Lubricating and Self-Healing Metals. Available online: https://www.researchgate.net/profile/Afsaneh_Dorri_Moghadam/publication/270510257_Synthesis_and_Properties_of_Metal_Matrix_Nanocomposites_MMNCS_Syntactic_Foams_Self_Lubricating_and_Self-Healing_Metals/links/54ac489a0cf2479c2ee7ac9a/Synthesis-and-Properties-of-Metal-Matrix-Nanocomposites-MMNCS-Syntactic-Foams-Self-Lubricating-and-Self-Healing-Metals.pdf (accessed on 18 March 2017).

17. Hassan, S.; Gupta, M. Development of nano–Y2O3 containing magnesium nanocomposites using solidification processing. *J. Alloy. Compd.* **2007**, *429*, 176–183. [CrossRef]

18. Sankaranarayanan, S.; Jayalakshmi, S.; Gupta, M. Effect of addition of mutually soluble and insoluble metallic elements on the microstructure, tensile and compressive properties of pure magnesium. *Mater. Sci. Eng. A* **2011**, *530*, 149–160. [CrossRef]

19. Braszczyńska-Malik, K. Some Mechanical Properties of Experimental Mg–Al–RE–Mn Magnesium Alloys. *Arch. Foundry Eng.* **2014**, *14*, 13–16. [CrossRef]

20. Greger, M.; Kocich, R.; Čížek, L.; Dobrzański, L.A.; Juřička, I. Possibilities of mechanical properties and microstructure improvement of magnesium alloys. *Arch. Mater. Sci. Eng.* **2007**, *28*, 83–90.

21. Moosa, A.A. Effect of Lanthanum Addition on the Microstructure of Mg–4Al Alloy. *Al-Khwarizmi Eng. J.* **2011**, *7*, 75–82.

22. Zhang, J.; Yu, P.; Liu, K.; Fang, D.; Meng, J. Effect of substituting cerium-rich mischmetal with lanthanum on microstructure and mechanical properties of die-cast Mg–Al–RE alloys. *Mater. Des.* **2009**, *30*, 2372–2378. [CrossRef]

23. Tekumalla, S.; Seetharaman, S.; Almajid, A.; Gupta, M. Mechanical properties of magnesium-rare earth alloy systems: A review. *Metals* **2014**, *5*, 1–39. [CrossRef]

24. Kainer, K.U.; Kaiser, F. *Magnesium Alloys and Technology*; John Wiley & Sons: Hoboken, NJ, USA, 2003.

25. Bai, J.; Sun, Y.; Xue, F. Microstructures and creep properties of Mg–4Al–(1–4) La alloys produced by different casting techniques. *Mater. Sci. Eng. A* **2012**, *552*, 472–480. [CrossRef]

26. Jain, C.C.; Koo, C.H. Creep behavior of extruded sheets of magnesium alloys containing La-rich Mischmetal. *Mater. Trans.* **2006**, *47*, 433–439. [CrossRef]

27. Kim, J.M.; Lee, S.J. Microstructure and Castability of Mg–Al–La Alloys for High Conductivity Applications. *Int. J. Met.* **2015**, *9*, 15–21. [CrossRef]

28. Zhang, J.H.; Zhang, M.L.; Meng, J.; Wu, R.Z.; Tang, D.X. Microstructures and mechanical properties of heat-resistant high-pressure die-cast Mg–4Al–*x*La–0.3Mn (*x* = 1, 2, 4, 6) alloys. *Mater. Sci. Eng. A* **2010**, *527*, 2527–2537. [CrossRef]

29. Zhang, J.H.; Liu, S.J.; Zhe, L.; Zhang, M.L.; Meng, J.; Wu, R.Z. Structure stability and mechanical properties of high-pressure die-cast Mg–Al–La–Y–based alloy. *Mater. Sci. Eng. A* **2012**, *531*, 70–75. [CrossRef]

30. Nguyen, Q.; Gupta, M. Increasing significantly the failure strain and work of fracture of solidification processed AZ31B using nano–Al2O3 particulates. *J. Alloy. Compd.* **2008**, *459*, 244–250. [CrossRef]

31. Yang, Q.; Bu, F.; Zheng, F.; Liu, X.; Zhang, D.; Qiu, X.; Meng, J. Influence of trace Sr additions on the microstructures and the mechanical properties of Mg–Al–La–based alloy. *Mater. Sci. Eng. A* **2014**, *619*, 256–264. [CrossRef]

32. Zhang, J.; Zhang, D.; Tian, Z.; Wang, J.; Liu, K.; Lu, H.; Tang, D.X.; Meng, J. Microstructures, tensile properties and corrosion behavior of die–cast Mg–4Al–based alloys containing La and/or Ce. *Mater. Sci. Eng. A* **2008**, *489*, 113–119. [CrossRef]

33. Wei, L.; Dunlop, G. The solidification behaviour of Mg–Al–rare earth alloys. *J. Alloy. Compd.* **1996**, *232*, 264–268. [CrossRef]

34. Zou, H.; Zeng, X.; Zhai, C.; Ding, W. Effects of Nd on the microstructure of ZA52 alloy. *Mater. Sci. Eng. A* **2005**, *392*, 229–234. [CrossRef]

35. Sankaranarayanan, S.; Nayak, U.P.; Stbat, R.K.; Suwas, S.; Almajid, A.; Gupta, M. Nano–ZnO particle addition to monolithic magnesium for enhanced tensile and compressive response. *J. Alloy. Compd.* **2014**, *615*, 211–219. [CrossRef]

36. Goodfellowc. Metals and Materials for Research and Industry. Alloys, and Ceramics Compounds. Available online: http://www.goodfellow.com/E/M.html (accessed on 14 March 2017).

37. Nguyen, Q.B.; Nai, M.L.S.; Nguyen, A.S.; Seetharaman, S.; Jayalakshmi, S.; Leong, E.W.W.; Gupta, M. Microstructure and damping characteristics of Mg and its composites containing metastable Al85Ti15 particle. *J. Compos. Mater.* **2016**, *50*, 2565–2573. [CrossRef]

38. Batra, R.C.; Wei, Z.G. Instability strain and shear band spacing in simple tensile/compressive deformations of thermoviscoplastic materials. *Int. J. Impact. Eng.* **2007**, *34*, 448–463. [CrossRef]

39. Wang, T.S.; Hou, R.J.; Lv, B.; Zhang, M.; Zhang, F.C. Microstructure evolution and deformation mechanism change in 0.98C–8.3Mn–0.04N steel during compressive deformation. *Mater. Sci. Eng. A* **2007**, *465*, 68–71. [CrossRef]